RESEARCH ARTICLE

Optimization of optical properties of toluene-core photonic crystal fibers with circle lattice for supercontinuum generation

Thuy Nguyen Thi[1] · Duc Hoang Trong[1] · Bao Tran Le Tran[2] · Trong Dang Van[2] ·
Lanh Chu Van[2]

Abstract We emphasize the advantage of varying the filling factor d_1/Λ in the first cladding ring of toluene-core PCFs with circle lattice in enhancing the fiber nonlinearity. The guiding characteristic of the fiber such as the dispersion, nonlinear coefficients, and attenuation of the fundamental mode is studied numerically. Based on the simulation results, two optimal PCFs are selected and investigated in detail for the spectrally broad supercontinuum (SC) generation with low input energy. The first PCF with a lattice constant (Λ) of 1.0 μm and filling factor (d_1/Λ) of 0.7 has the all-normal dispersion in the wavelength range of 0.7–2.0 μm. When the 1-cm-long fiber samples are pumped at 1.064 μm, the generated SC spectra span from the visible to near-infrared regions (0.642–1.592 μm), with the low pulse energy of 0.018 nJ. Meanwhile, the second PCF (Λ = 2.5 μm, d_1/Λ = 0.3) allows for SC in the anomalous dispersion regime in the range 0.911–2.496 μm with pulse energy of 0.05 nJ when the pulse has a central wavelength of 1.55 μm propagating within 10 cm of the fiber samples. The proposed design could be a new class of microstructure optical fiber for the broad spectrum SC generation.

Keywords Toluene-core photonic crystal fibers ·
Supercontinuum generation · All-normal dispersion ·
Anomalous dispersion · The filling factor d_1/Λ · The first
cladding ring

✉ Lanh Chu Van
  chuvanlanh@vinhuni.edu.vn

[1] University of Education, Hue University, 34 Le Loi Street,
   Hue City, Viet Nam

[2] Department of Physics, Vinh University, 182 Le Duan,
   Vinh City, Viet Nam

Introduction

SC generation is a complex nonlinear phenomenon where laser light is converted to light with an intense ultra-broadband through a strongly nonlinear device [1–4]. Photonic crystal fibers (PCFs) have two properties that make them an excellent medium for generating SC: customizable dispersion and strong-mode confinement. That can allow a strong nonlinear interaction over a significant length of the fiber [5–7]. Many publications with some common solutions have presented ways to design PCFs to enhance their nonlinear properties as variation of the geometrical parameters of the lattice [8–13] and using liquids to infiltrate into the air hole or the core of the PCFs.

In recent years, SC generation in liquid-core PCFs has been extensively studied due to the outstanding advantages of liquids such as high nonlinear and tunable properties. The enhancement of nonlinearity properties in liquid-core PCFs makes the SC spectral broader with a lower energy of pump pulses and shorter fiber length. Moreover, the flat dispersion profile, high nonlinear coefficient, and low attenuation of PCF are also very important keys for generating the flatter, and smoother SC spectrum with the same laser parameters. Many different liquids have been used to fill the air holes or hollow cores of PCF such as chloroform [14–18], carbon disulfide [18–20], carbon tetrachloride [21–25], tetrachloroethylene [26], nitrobenzene [27, 28], benzene [29, 30], ethanol [31], methanol [32], isopropanol [33], water, and oil, etc., [34–40] which can effectively control the dispersion characteristics, nonlinear coefficient, and attenuation of the fundamental mode. At the same time, by varying the core diameter (D_c), the lattice constant (Λ), and the filling factor (d/Λ) of the lattice, the liquid-core PCFs can be controlled to obtain all-normal and anomalous dispersion characteristics.

Typically, the soliton fission and modulation instability based on the controlled anomalous and all-normal dispersion properties in PCFs are two common mechanisms to achieve SC generation. Soliton fission will prevail in the anomalous dispersion regime, i.e. the PCF exists zero wavelength dispersion (ZDW). A board SC spectrum can be generated with low input power but still noise due to the sensitivity of the solution to pump pulse vibrations, while the modulation instability through the self-phase modulation (SPM) and optical wave-breaking (OWB) takes to control the SC generation process with PCF having all-normal dispersion characteristic. The phase coherence of the generated SC pulses can be very high, even under conditions of strong spectral broadening, but the input energy must be high [5, 41–46]. In many works, thanks to skillful adjustment of lattice parameters such as D_c, Λ, and d/Λ, the SC spectrum expansion from the visible to near-infrared regions in all-normal dispersion [15, 24, 28], anomalous dispersion [14, 19, 23] or both all-normal and anomalous dispersion regime [16, 22, 26, 27] with the same type liquid that infiltrates the PCFs, is announced theoretically as well as experimentally.

Because toluene (C_7H_8) has a high nonlinear refractive index, relatively low attenuation concerning the other nonlinear liquids [47], and low toxicity, it has been also chosen as an excellent liquid to infiltrate the PCF is used for SC generation. The nonlinear refractive index of C_7H_8 is $n_2 = 16 \times 10^{-19}$ m$^2 \cdot$W^{-1} at the wavelength of 1.064 μm. It is 60 times higher compared to silica ($n_2 = 2.74 \times 10^{-2}$ m$^2 \cdot$W^{-1}) [48]. SC generation in the visible range with a toluene-filled core PCF was shown by Fanjoux et al. [49]. It operates in the strong normal dispersion regime, but the input pulse energy was high (200 nJ); the SC spectrum extended from 0.55 to 0.87 μm with a pump wavelength of 0.532 μm. Hoang et al. [50] measured SC generation in all-normal dispersion of PCFs with large hollow cores infiltrated with toluene, the broad spectrum covers a wavelength range of 0.95–1.10 μm for the 10 nJ incident pulse energy, and the nonlinear coefficient of 130 W$^{-1} \cdot$km^{-1} was obtained at 1.03 μm. SC with both all-normal and anomalous dispersion has generated over the range of 1.0–1.7 μm, reported by Lanh et al. [51]; however, in this case, the confinement losses in the considered structures are as high as 0.4 dB/cm. Besides, toluene-filled photonic crystal fiber with flat dispersion and low confinement loss for designing a refractive index sensor was performed by Sharma et al. [52]. Qui et al. [53] and Yashar et al. [54] also introduced an all-solid cladding dual-core PCF filled with toluene which is proposed for temperature sensing.

Although the role of toluene in improving the dispersion characteristics of PCF has been mentioned, the simultaneous optimization of three characteristic quantities such as dispersion characteristic, nonlinear coefficients, and attenuation for SC generation has not been surveyed. In this paper, we proposed the new PCF filled with toluene by adjusting the filling factor d_1/Λ in the first cladding ring with circle lattice in enhancing the fiber nonlinearity. First, the nonlinear characteristic is numerically investigated to find the optimal structures with flat dispersion, high nonlinear coefficients, and low attenuation. Second, the spectral width over 1.0 μm with a rather small input pulse energy of SC generation with two selected structures in all-normal and anomalous dispersion regime are analyzed in detail. We choose the circular lattices PCF structure because of its high symmetry; it confines light tightly to the core and increases nonlinearity and hence the SC generation efficiency, i.e. better bandwidth enhancement compared to other lattices.

Numerical modeling of the toluene-core PCFs

The schematic view of the geometrical structure of the modelled C_7H_8-filled PCF has displayed in Fig. 1. It consists of 8 rings of air-holes ordered in a circle lattice, the linear filling factor of the cladding has defined by the ratio d/Λ, where d is the diameter of a single air-hole, and Λ is the lattice constant. We assume that PCF has made of fused silica glass (SiO_2) and the central hole filled with C_7H_8. The work [55] shows that the diameter of the air holes in the first ring surrounding the core has a major influence on controling dispersion properties including flatness and zero-dispersion wavelength shift. Meanwhile, the attenuation of the fundamental mode and even the higher modes is strongly dominated by the size of subsequent rings. Thus, in our simulation, the air holes diameter of the second ring onwards of the cladding has the same value, but the air holes diameter of the first ring near the core is varied to
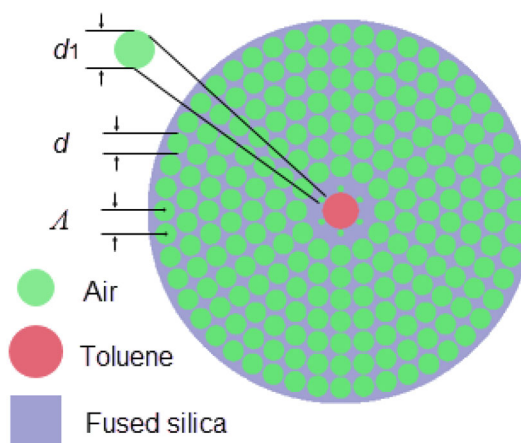

Fig. 1 The geometrical structures of PCF with toluene-core

control the nonlinearity properties of PCFs (note that, the works [49–53] do not indicate differences in the air hole diameter of rings). We use the following lattice constants Λ: 1.0 μm, 1.5 μm, 2.0 μm, and 2.5 μm, the filling factor d_1/Λ of the first ring is varied from 0.3 to 0.8, and the filling factor d/Λ of the second and other rings is constant of 0.95. The core whose diameter is determined by the formula $D_c = 2\Lambda - 1.2d_1$ has the smallest and the largest value of 1.04 μm and 4.64 μm, respectively, for cases $\Lambda = 1$ μm, $d_1/\Lambda = 0.8$ and $\Lambda = 2.5$ μm, $d_1/\Lambda = 0.3$.

Sellmeier's equation [56] shows the dependence of refractive index characteristics on wavelength for toluene:

$$n_{\text{Toluene}}^2(\lambda) = 2.161659124 + 0.000495188\lambda^2$$
$$+ \frac{0.021381790}{\lambda^2} + \frac{0.000058838}{\lambda^4}$$
$$+ \frac{0.000087632}{\lambda^6} \quad (1)$$

With the fused silica, the refractive index can be obtained using the Sellmeier formula [57]:

$$n_{\text{Fusedsilica}}^2(\lambda) = 1 + \frac{0.6694226\lambda^2}{\lambda^2 - 4.4801 \times 10^{-3}}$$
$$+ \frac{0.4345839\lambda^2}{\lambda^2 - 1.3285 \times 10^{-2}} + \frac{0.8716947\lambda^2}{\lambda^2 - 95.341482} \quad (2)$$

where λ is the excitation wavelength in micrometers; $n(\lambda)$ is the wavelength-dependent linear refractive index of materials.

The real parts of refractive index of toluene and fused silica used in this paper versus wavelength are shown in Fig. 2. To create C_7H_8-filled PCF, we used the commercial Lumerical Mode Solution (LMS) [58]. First, it is necessary to put data on the refractive index and loss of C_7H_8 into the material database of LMS. Next, we create the SiO_2 base material in structures and choose a hollow-core circular lattice in the photonic crystal. Finally, C_7H_8 is put into the
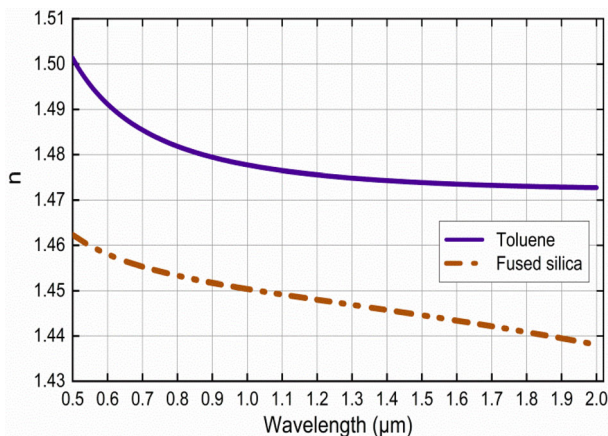

Fig. 2 Real parts of refractive index of toluene and fused silica

hollow core of the PCF. We limited the simulation for the wavelength range of 0.7–2.0 μm since reliable data are available only in this range. By using the finite-difference eigenmode (FDE) method, the characteristic properties of C_7H_8-filled PCF are simulated with the assumption that toluene exhibits significant losses. The process of FDE utilizes the Maxwell wave equation, and the boundary condition is the perfectly matched layers to analyze the structure makes no reflection at the boundary and reduces the loss. In addition, FDE divides the cross section of the fiber into smaller rectangular sections of a hundred thousand parts to increase the numerical accuracy of the simulations.

## Dispersion properties of the toluene-core PCFs

We have calculated numerically the dispersion coefficient of the toluene-core PCFs including both waveguide and materials dispersion using the real part of the effective index from the following formula:

$$D = -\frac{\lambda}{c} \frac{d^2 \text{Re}[n_{\text{eff}}]}{d\lambda^2} \quad (3)$$

where $\text{Re}[n_{\text{eff}}]$ is the real part of n_{eff} which is the effective index of a guided mode calculated by means FDE method and c is the velocity of light in a vacuum.

Figure 3 depicts that the dispersion depends on wavelength for different values of the filling factor d_1/Λ and the lattice constants Λ. The decrease in the filling factor reduces the dispersion profile for all values of the lattice constant. With a small lattice constant ($\Lambda = 1.0$ μm, Fig. 3a), PCFs exhibit both anomalous and normal dispersion properties with a larger shift of ZDWs towards the longer wavelength region. PCFs with two ZDWs are obtained when d_1/Λ is equal to 0.8 and 0.75; meanwhile, the PCF with only one ZDW is found with smaller d_1/Λ (from 0.3 to 0.4) in the investigated wavelength region. In the rest cases, the dispersion is completely located in the normal dispersion, increasing the values of the filling factor d_1/Λ (0.45 to 0.7) making the all-normal dispersions more and more flat and close to the zero-dispersion line. Specifically, the dispersion is flattest and closest to the zero dispersion for the PCF with $d_1/\Lambda = 0.7$. Figure 3a also exposes that the slope of the dispersion changes drastically for a variation of air-hole diameter, i.e. the change of the filling factor. The effect can be explained based on the interaction between waveguide dispersion and material dispersion. For smaller d_1/Λ, matter dispersion plays a major role while waveguide effect dominates for larger d_1/Λ. Besides, varying Λ influences the dispersion properties of PCF; this is denoted in Fig. 3b, c, and d. The value of dispersion has changed because of the increase of Λ

Fig. 3 a The dispersion characteristics of toluene-core PCFs with various values of d_1/Λ and $\Lambda = 1.0$ μm **b** The dispersion characteristics of toluene-core PCFs with various values of d_1/Λ and $\Lambda = 1.5$ μm. **c** The dispersion characteristics of toluene-core PCFs with various values of d_1/Λ and $\Lambda = 2.0$ μm. **d** The dispersion characteristics of toluene-core PCFs with various values of d_1/Λ and $\Lambda = 2.5$ μm
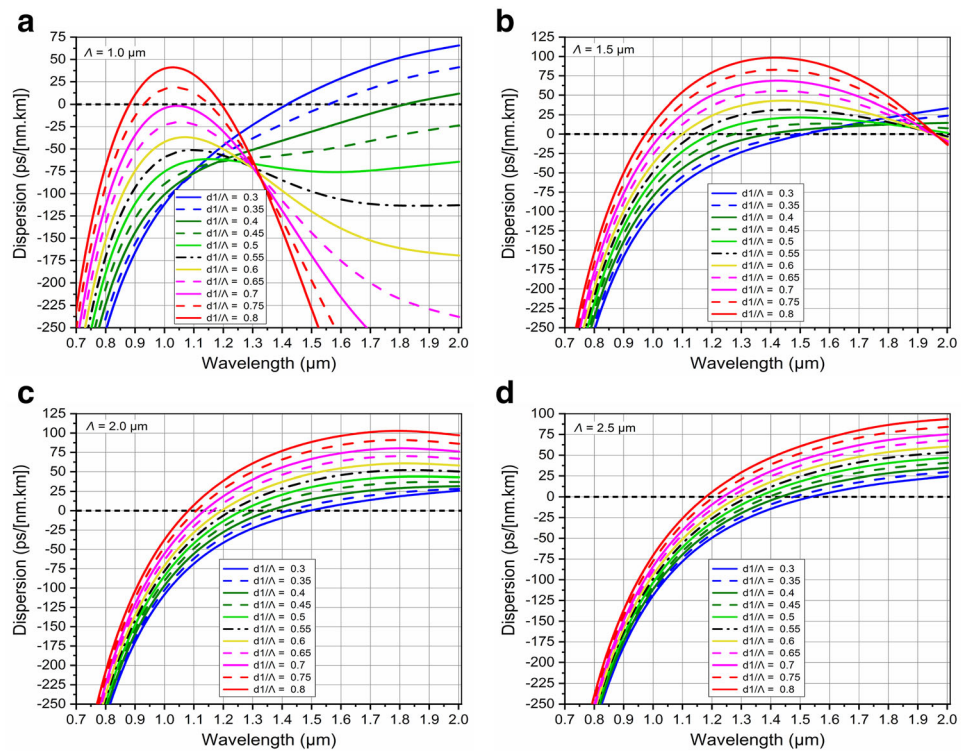
without much change in slope. All dispersions operate in the anomalous dispersion regime with the existence of ZDWs when $\Lambda \geq 1.5$. Furthermore, the ZDWs move towards longer wavelengths gradually as the Λ increase because of the predominance of material dispersion, the values of ZDW are presented in Table 1. Shifting the ZDW toward longer wavelengths in PCFs has an important role for soliton-driven supercontinuum by low cost and short pulse lasers with the pump wavelength chosen to be larger but closer to ZDW. For $\Lambda = 2.0$ and 2.5 μm, the dispersion curves have only one ZDW, in the case, $\Lambda = 2.5$ μm and $d_1/\Lambda = 0.3$, the value of ZDW is 1.536 μm, which is very

approximate to the common pump wavelength in SC generation-based silica-PCF.

Figure 3 verifies that the decisive factor effect upon dispersion is the infiltration of the toluene into the core and the variation of the lattice parameters in the first ring surrounding the core, making the dispersion and the slope change drastically. The change in the optical pulse per unit distance of the propagation length of the fiber is caused by dispersion, so a PCF with suitable dispersion properties for SC generation is an essential element. Usually, the PCF has an all-normal and flat dispersion being necessary for expansion spectrum in SC generation in the visible and

Table 1 The values of ZDW of toluene-core PCFs with various values of d_1/Λ and Λ

d_1/Λ	$\Lambda = 1.0$ μm		$\Lambda = 1.5$ μm		$\Lambda = 2.0$ μm	$\Lambda = 2.5$ μm
	ZDWs$_1$	ZDWs$_2$	ZDWs$_1$	ZDWs$_2$	ZDWs	ZDWs
0.3	1.423	–	1.529	–	1.501	1.536
0.35	1.568	–	1.499	–	1.422	1.481
0.4	1.811	–	1.399	–	1.364	1.435
0.45	–	–	1.277	–	1.306	1.394
0.5	–	–	1.201	–	1.264	1.361
0.55	–	–	1.143	1.983	1.223	1.324
0.6	–	–	1.098	1.978	1.195	1.297
0.65	–	–	1.064	1.962	1.164	1.268
0.7	–	–	1.032	1.960	1.139	1.237
0.75	0.926	1.167	1.003	1.966	1.113	1.210
0.8	0.882	1.202	0.977	1.967	1.089	1.184

near-infrared regions. Meanwhile, the low anomalous dispersion near ZDW provides the generation of a broad supercontinuum with strong confinement to the core despite the low input energy [34]. Moreover, the shift of the ZDW to the longer wavelength and flat dispersion suggests that we can use available lasers with femtosecond optical pulses as input sources for coherent SC generation. Based on the preliminary studies on the influence of lattice parameters on dispersion, we proposed two optimal PCFs to be beneficial to generate SC, namely $\#F_1$ and $\#F_2$. Both the introduced PCF structures provide reasonable flatness dispersion and are close to the zero-dispersion curve in the investigated wavelength region, as presented in Fig. 4. The first fiber $\#F_1$ has the following structure parameters: $\Lambda = 1.0$ µm and $d_1/\Lambda = 0.7$, which is used for SC generation in all-normal dispersion regime with 1.064 µm of the pump wavelength with the expectation of reaching the broad spectrum because of the nearness of the pump wavelength to a local maximum of dispersion curve, while the second fiber $\#F_2$ ($\Lambda = 2.5$ µm and $d_1/\Lambda = 0.3$) has the anomalous dispersion, which is expected to generate broad-spectrum SC with the pump wavelength of 1.55 µm because its ZDW is equal to 1.537 µm, closest to the pump wavelength. Another way, the dispersion of this fiber is the flattest for all dispersion characteristics with $\Lambda = 2.5$ µm; this is also a decisive factor to be noticed in SC generation. It should be noted that the action of increasing the core diameter of the PCF has also strongly influenced the SC generation because increasing the core diameter will increase the effective mode area and ultimately reduce the nonlinear coefficient. Because the dispersion of the two proposed fibers at the pump wavelength is quite small, we expect that this small dispersion value is beneficial to the spectral expansion despite the high dispersion slope. The

structural parameters of the two proposed PCFs are shown in Table 2.

Other nonlinear optical properties of two selected structures are also investigated in detail. Figure 5 illustrates the numerical results of the effective mode area on the wavelength of these structures. As the wavelength increases, the light is no longer confined strongly inside the core because the modes get leaked through the holes, in between them increasing the effective mode area. With the larger lattice constant and the larger diameter $\#F_2$ fiber has a larger effective mode area than that of $\#F_1$ fiber. If the effective mode area increases, the higher-order modes will be allowed to enter the fiber core; therefore, we always keep in mind the limit of increasing the diameter of the fiber core in the process of optimizing the properties of PCFs. The effective mode area for the fundamental mode of fibers $\#F_1$ is 1.221 µm^2 for a pump wavelength of 1.064 µm, while that of $\#F_2$ fiber is 10.497 µm^2 at 1.55 µm pump wavelength; these values are much smaller than some previous publications of PCF with toluene infiltration [50, 51].

The nonlinear coefficient γ is calculated through the following equation using the effective area value in each wavelength: $\gamma = \omega_0 n_2/cA_{\text{eff}}$, where n_2 is the nonlinear refractive index coefficient of silica, c is the velocity of light, and ω_0 is the central frequency of the pulse. The nonlinear coefficient of the proposed PCFs is presented in Fig. 6. The nonlinear coefficient of the fibers rises along with the decrease of the effective mode area. As expected, the alteration of the filling factor and the lattice constant significantly improves the nonlinearity coefficient of fibers. The nonlinear coefficient of $\#F_1$ and $\#F_2$ is 7827.614 W^{-1}·km^{-1} at 1.064 µm and 899.836 W^{-1}·km^{-1} at 1.55 µm, respectively.

Figure 7b evinces the attenuation characteristics of the fundamental mode for $\#F_1$ and $\#F_2$ fiber. The losses analysis showed that the attenuation of fundamental modes for proposed $\#F_1$ is 0.08 dB/cm at 1.064 µm; this value is equal to 2.025 dB/cm for $\#F_2$ at 1.55 µm. The reason of the low value of attenuation for the fundamental mode of our design is that the mode is well confined in the core; majority of electromagnetic field is located there and the losses introduced by toluene are not mostly affected [51].
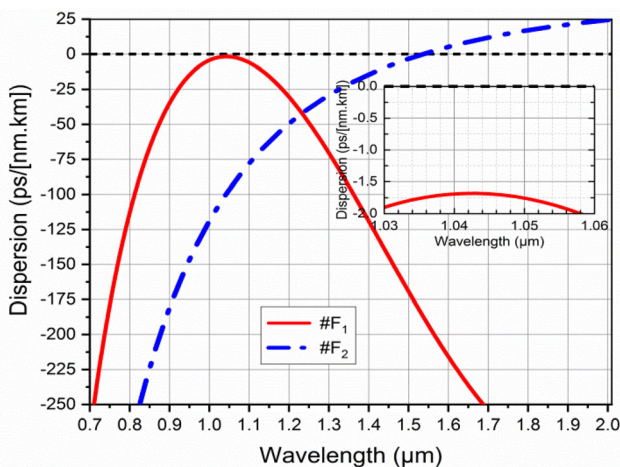

Fig. 4 The dispersion characteristics of the fundamental mode for $\#F_1$ and $\#F_2$ fiber

Table 2 The structure parameters of proposed PCFs

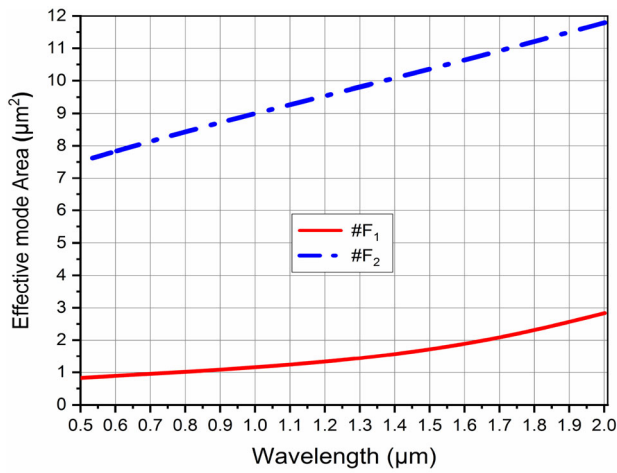| #	D_c (µm)	Λ (µm)	d_1/Λ	D (ps·nm^{-1}·km^{-1})
$\#F_1$	1.16	1.0	0.7	− 0.557
$\#F_2$	4.64	2.5	0.3	1.502

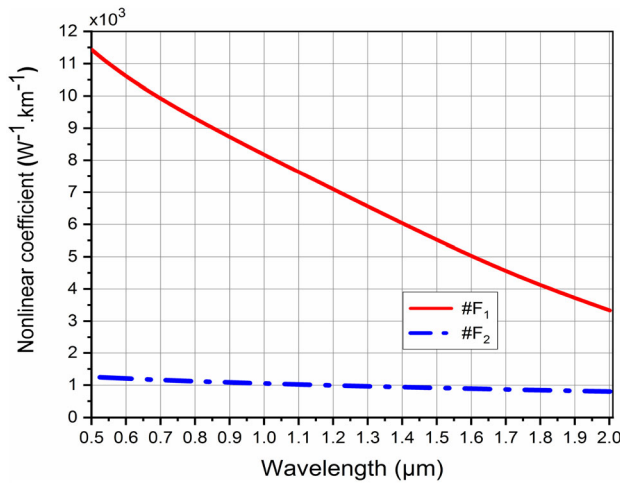**Fig. 5** The effective mode area of the fundamental mode for #F$_1$ and #F$_2$ fiber

Fig. 6 The nonlinear coefficient of the fundamental mode for #F$_1$ and #F$_2$ fiber
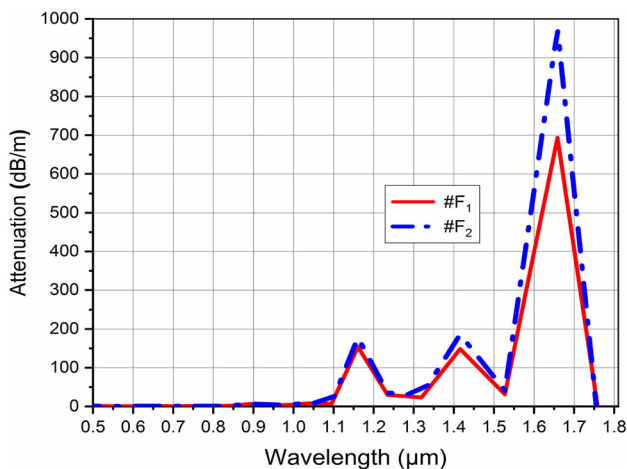

Fig. 7 The attenuation of the fundamental mode for #F$_1$ and #F$_2$ fiber

Thanks to the difference in the design of the structural parameters of the first ring near the core and the others, and the toluene infiltration into the core of PCF with circular lattice, we achieve the optimal dispersion, high nonlinearity, low attenuation as expected. Those are the interesting features of our proposed PCFs that are beneficial for SC generation.

Supercontinuum generation in proposed fiber

The nonlinear properties analyzed above show great potential to generate SC for the proposed toluene-filled PCFs. The refractive index of the medium is changed drastically due to the infiltration of toluene into the core leading to the nonlinear effects in SC generation. The nonlinear propagation process of the pump pulse in the PCF can be described by the Schrödinger equation (GNLSE) using the symmetry split-step Fourier transform method [59], given by the formula:

$$\partial_z A - i\,\widetilde{\beta}(\omega)\,A - \frac{\widetilde{\alpha}(\omega)}{2}\,A = i\gamma\left(1 + \frac{\omega - \omega_0}{\omega_0}\right)A\mathbb{F}$$
$$\left[\int_{-\infty}^{\infty} R(T')|A|^2(T - T')dT'\right] \tag{4}$$

where $A(z, \omega)$ is Fourier transform of the amplitude of a pulse $A(z, T)$, and $R(T')$ is the Raman response function. The left side of Eq. (4) depicts the linear propagation effects of the fiber; $\widetilde{\alpha}$ and $\widetilde{\beta}$ are attenuation and dispersion in the frequency domain, respectively. In our numerical modeling, the high-order dispersions are calculated through the development coefficients of the Taylor series of the circulation constant at the pumping pulse frequency. The high order of dispersion is shown in Table 3.

Table 3 The coefficient of high-order dispersion at the pump wavelength

Coefficients	#F$_1$	#F$_2$
β_2 (ps^2/m)	2.32×10^{-3}	-1.88×10^{-3}
β_3 (ps^3/m)	-1.67×10^{-5}	1.41×10^{-4}
β_4 (ps^4/m)	5.97×10^{-7}	-2.56×10^{-7}
β_5 (ps^5/m)	-3.94×10^{-9}	1.17×10^{-9}
β_6 (ps^6/m)	2.39×10^{-11}	9.44×10^{-13}
β_7 (ps^7/m)	3.33×10^{-13}	-1.47×10^{-13}
β_8 (ps^8/m)	-5.15×10^{-15}	-7.29×10^{-16}
β_9 (ps^9/m)	-1.14×10^{-16}	3.83×10^{-17}
β_{10} (ps^{10}/m)	2.21×10^{-18}	1.19×10^{-18}
β_{11} (ps^{11}/m)	2.43×10^{-20}	-3.80×10^{-20}

The evolution of SC spectra as a function of input pulse energy set up in the range 0.003–0.018 nJ shown in Fig. 8. In our numerical simulations, fiber #F1 has a propagation length of 1 cm, is pumped at the center wavelength of 1.064 μm, and has a pulse duration of 40 fs chosen. The main effect that plays an important role in spectral broadening is the self-phase modulation (SPM) followed by optical wave breaking (OWB) because #F1 fiber has the all-normal dispersion regime. When the input pulse energy is low (0.003 nJ), the pump pulse is broadened by SPM, the SPM-induced spectrum has many peaks and the outermost peak has the most intense. In this case, the achieved spectral broadening is very limited due to the existence of only the SMP process. As the pulse energy has increased (higher than 0.003 nJ), SPM is the cause of spectral broadening at the beginning of propagation, and then OWB dominates the spectral broadening at the wings by four-wave mixing (FWM) [24, 51]. The OWB effect starts to occur at a wavelength of 0.75 μm when the input energy is 0.006 nJ, with the further increase of the input pulse energy; this effect appears at a shorter wavelength (Fig. 8a).

Figure 8b–c displays the continuous broadening of the pulse in the temporal domain. When the input pulse energy is higher than 0.003 nJ, initial development of spectrum is induced by SPM in the vicinity of the central wavelength, and then the spectrums are broadened considerably at the wings because of the onset of OWB, which exhibits the blue-shifted (trailing) edge and the red-shifted (leading) edge of the pulse [60], (Fig. 8b). In the case of input pulse energy of 0.018 nJ, the SC spectrum has broadened after the first few millimeters of pulse propagation because of the dominant contribution of SPM. The asymmetry of the generated spectrum toward the short wavelength range is due to the effects of nonlinear dispersion, e.g., self-steepening. The new short-wavelengths generated by SPM at the trailing edge experiences effects of the dispersion move slower than the pulse tail at the center of the pulse. The interference of the pulse tail and the slower wavelengths leads to the onset of OWB, and the newly wavelengths can be created via four-wave mixing (FWM) [24, 50]. At the trailing edge of the pulse, OWB occurred and the newly generated wavelengths around 0.65 μm appear at a propagation distance of about 2 mm. During further propagation, spectral broadening at the trailing edge of the pulse is
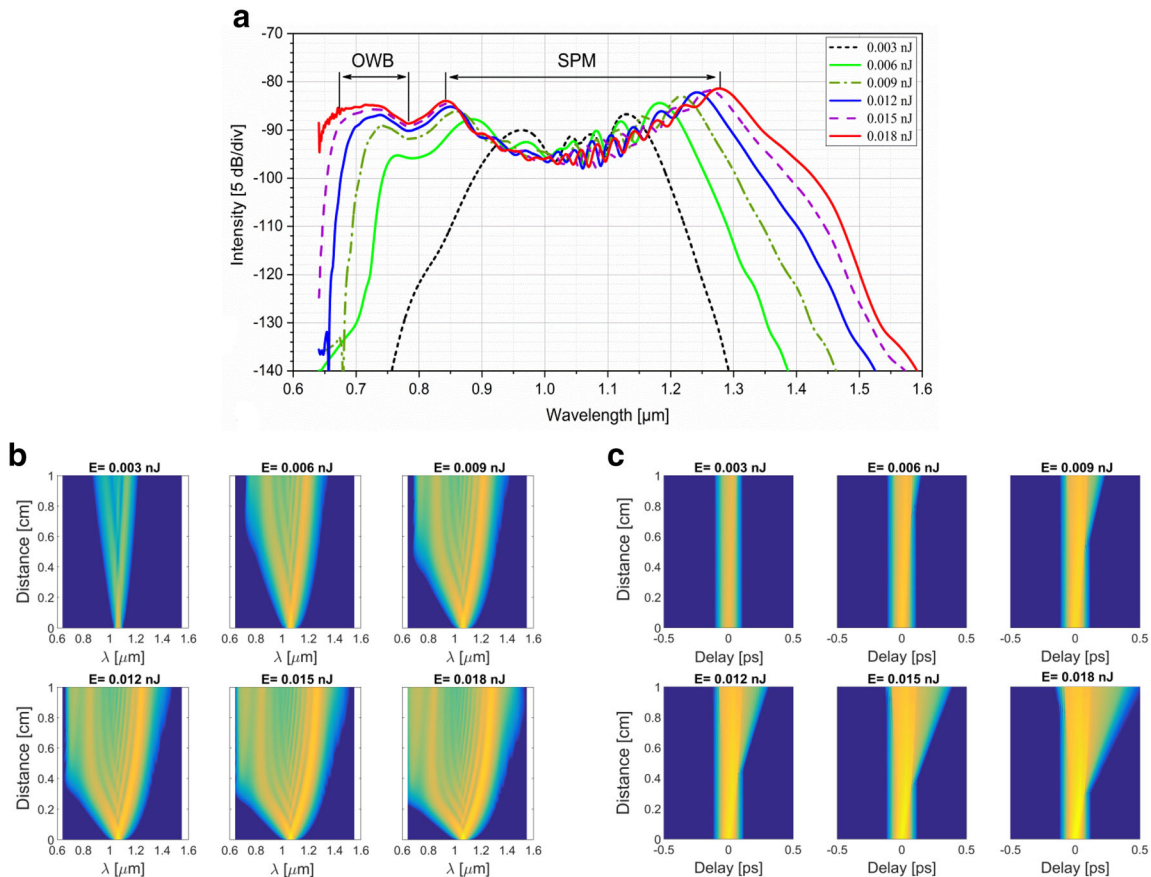

Fig. 8 For #F1 fiber: **a** various input pulse energy in 1 cm length when pumped with pulses of 40 fs duration, 1.064 μm pump wavelength, **b** the evolution of the SC along with fiber, **c** the temporal profile at various propagation length

restricted by the high slope of dispersion. At the leading edge of the pulse, the large effective mode area and high attenuation of the fiber in the long-wavelength band limit the spectral broadening [27, 51]. The broadest SC spectrum covers from 0.642 to 1.592 μm of the wavelength within the 5 dB dynamic range.

The input pulse energies range from 0.001 to 0.05 nJ at pump wavelength 1.55 μm, injected into #F_2 fiber of length 10 cm in a 10 dB dynamic range, and the pulse duration is 90 fs. The SC spectrum depends on the input energy illustrated in Fig. 9a. Because #F_2 fiber operates in the anomalous dispersion regime pumping, the spectral broadening leading to SC is typically governed by the soliton dynamics, e.g. soliton fission (SF), self-frequency shifting [5]. In principle, the injected higher-order soliton tends to split when its bandwidth reaches a maximum, both the higher-order dispersion and Raman scattering account to perturbation and thereby contribute to SF [21, 39]. When the fiber is pumped in the low energy region 0.001–0.01 nJ, the bandwidth is very small because SPM plays a dominant role in spectral broadening, this phenomenon is similar to the #F_1 fiber. As the input energy increases (0.03 and

0.05 nJ), the SF begins to show its influence to broaden the spectrum.

As can be seen from Fig. 9b and c, when the input energy reaches its maximum of 0.05 nJ, the main contribution of SPM makes the spectrum broad at the beginning of the propagation. SF occurs around 3 cm of propagation, and the solitons would shift toward the longer wavelengths due to soliton self-frequency shifts [5], leading to spectral broadening toward the side of red light and generating new wavelength components up to 2.5 μm (across the ZWD) at the leading edge and around 1.3 μm at the trailing edge. [27]. The achieved bandwidth is about 1.585 μm spanning the region from 0.911 to 2.496 μm of the wavelength within the 10 dB dynamic range.

Table 4 summarizes the achieved SC performance in comparison with other SC based on PCF with various liquid infiltration. Our proposed toluene core-PCFs show outstanding advantages such as the flat dispersion, high nonlinearity, and low attenuation as expected to generate a broader spectrum with very low energy laser pulses, which enhances the efficiency in SC.
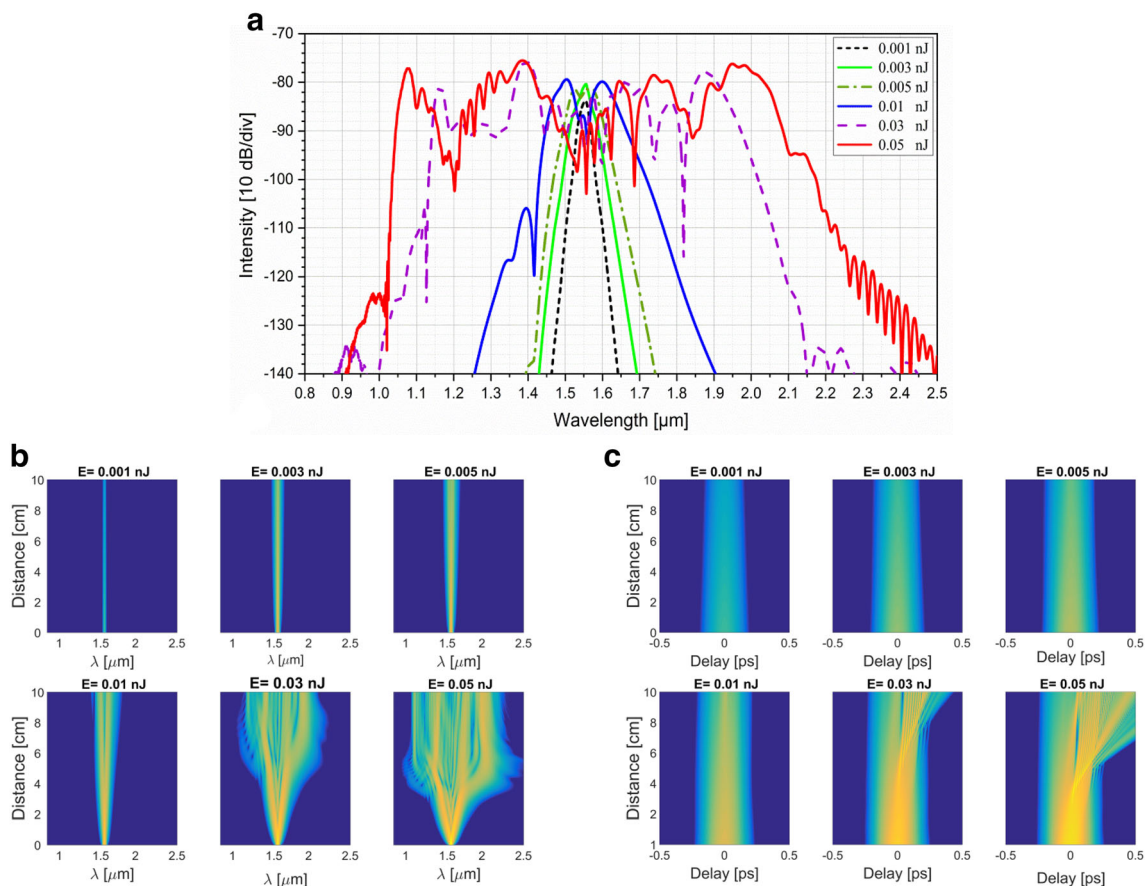

Fig. 9 For #F2 fiber: **a** various input pulse energy in 10 cm length when pumped with pulses of 90 fs duration, 1.55 μm pump wavelength, **b** the evolution of the SC along with fiber, **c** the temporal profile at various propagation length

Table 4 The SC generated in the proposed toluene core-PCF in comparison with other recent PCF designs

Liquid	τ (fs)	E (nJ)	Fiber length (cm)	λp (μm)	SC range (μm)	Regime	References
$CHCl_3$	100	5	10	1.06	0.365–1.315	Normal	[15]
$CHCl_3$	400	25	20	1.03	0.85–1.25	Normal	[17]
CS_2	30	0.32	30	1.59	1.1–2.2	Anomalous	[19]
CCl_4	300	0.8	30	1.064	0.95–1.15	Normal	[22]
CCl_4	400	25	20	1.03	0.85–1.25	Normal	[24]
C_2Cl_4	90	1.5	10	1.56	0.6–1.26	Anomalous	[26]
$C_6H_5NO_2$	90	0.5	5	1.56	0.8–2.1	Normal	[27]
C_2H_5OH	80	4	20	1.55	0.9–1.845	Anomalous	[29]
C_7H_8	400	10	10	1.03	0.95–1.1	Normal	[50]
C_7H_8	350	2.5	5	1.55	1.1–1.75	Normal	[51]
C_7H_8 (#F_1)	40	0.018	1	1.064	0.642–1.592	Normal	The present work
C_7H_8 (#F_2)	90	0.05	10	1.55	0.911–2.496	Anomalous	The present work

Conclusion

In this work, the SC generation broad spectrum in the visible and near-infrared region with a circular lattice photonic crystal fiber made of fused silica with the core infiltrated with toluene is numerically proposed and analyzed. Two optimal fibers #F_1 and #F_2 with $\Lambda = 1.0$ μm, $d_1/\Lambda = 0.7$ and $\Lambda = 2.5$ μm, $d_1/\Lambda = 0.3$ are selected to generate SC. #F_1 fiber has a normal dispersion profile, pumped at 1.064 μm central wavelength which generates a spectral bandwidth spanning from 0.642 to 1.592 μm due to the main contribution of SPM and OWB. The soliton fission governs the ability of spectral broadening in the anomalous dispersion regime of #F_2 fiber; the SC spectrum from 0.911 to 2.496 μm at 10-cm-long sample is obtained. Such a broad spectrum can achieve with low input energy because the difference of structural parameters in the first and other rings of the cladding leads to high nonlinearity, low attenuation, and flat dispersion of the PCF. The proposed model is designed, which can be a new class of fibers for all-fiber SC sources as an alternative to glass core fibers for the next generation of broad bandwidth sources.

References

1. A.M. Zheltikov, Let there be white light: supercontinuum generation by ultrashort laser pulses. Phys. Uspekhi **49**(6), 605 (2006). https://doi.org/10.1070/PU2006v049n06ABEH005975
2. W.J. Wadsworth, A. Ortigosa-Blanch, J.C. Knight, T.A. Birks, T.P.M. Man, P.S.J. Russell, Supercontinuum generation in photonic crystal fibers and optical fiber tapers: a novel light source. J. Opt. Soc. Am. B **19**(9), 2148–2155 (2002). https://doi.org/10.1364/JOSAB.19.002148
3. K. Nithyanandan, R.V.J. Raja, K. Porsezian, Power play in the supercontinuum spectra of saturable nonlinear media. Laser Phys. **24**(4), 045405 (2014). https://doi.org/10.1088/1054-660X/24/4/045405
4. G. Genty, S. Coen, J.M. Dudley, Fiber supercontinuum sources (Invited). J. Opt. Soc. Am. B **24**(8), 1771–1785 (2007). https://doi.org/10.1364/JOSAB.24.001771
5. J.M. Dudley, G. Genty, S. Coen, Supercontinuum generation in photonic crystal fiber. Rev. Mod. Phys. **78**, 1135 (2006). https://doi.org/10.1103/RevModPhys.78.1135
6. T. Schreiber, J. Limpert, H. Zellmer, A. Tünnermann, K.P. Hansen, High average power supercontinuum generation in photonic crystal fibers. Opt. Commun. **228**(1–3), 71–78 (2003). https://doi.org/10.1016/j.optcom.2003.09.091
7. W.J. Wadsworth, A. Ortigosa-Blanch, J.C. Knight, T.A. Birks, T.P. Martin Man, P.J. Russell, Supercontinuum generation in photonic crystal fibers and optical fiber tapers: a novel light source. J. Opt. Soc. Am. B **19**(9), 2148–2155 (2002). https://doi.org/10.1364/JOSAB.19.002148
8. S.E. Kim, B.H. Kim, C.G. Lee, S. Lee, K. Oh, C.S. Kee, Elliptical defected core photonic crystal fiber with high birefringence and negative flattened dispersion. Opt. Express **20**(2), 1385–1391 (2012). https://doi.org/10.1364/OE.20.001385
9. A. Sharafali, K. Nithyanandan, K. Porsezian, Self-similar pulse compression by defective core photonic crystal fiber with cubic-quintic nonlinearities. Optik **178**(4), 591–601 (2019). https://doi.org/10.1016/j.ijleo.2018.09.183
10. B.W. Liu, M.L. Hu, X.H. Fang, Y.F. Li, L. Chai, C.Y. Wang, W. Tong, J. Luo, A.A. Voronin, A.M. Zheltikov, Stabilized soliton self-frequency shift and 0.1-PHz sideband generation in a photonic-crystal fiber with an air-hole-modified core. Opt. Express **16**(19), 14987–14996 (2008). https://doi.org/10.1364/OE.16.014987
11. S. Roy, P.R. Chaudhuri, Supercontinuum generation in visible to mid-infrared region in square-lattice photonic crystal fiber made from highly nonlinear glasses. Opt. Commun. **282**(17), 3448–3455 (2009). https://doi.org/10.1016/j.optcom.2009.05.062
12. R. Ahmad, M. Komanec, S. Zvanovec, Circular lattice photonic crystal fiber for Mid-IR supercontinuum generation. IEEE Photonics Technol. Lett. **28**(23), 2736–2739 (2016). https://doi.org/10.1109/LPT.2016.2615657
13. M. Klimczak, D. Michalik, G. Stępniewski, T. Karpate, J. Cimek, X. Forestier, R. Kasztelanic, D. Pysz, R. Stępień, R. Buczyński, Coherent supercontinuum generation in tellurite glass regular

lattice photonic crystal fibers. J. Opt. Soc. Am. B **36**(2), A112–A124 (2019). https://doi.org/10.1364/JOSAB.36.00A112

14. H. Zhang, S. Chang, J. Yuan, D. Huang, Supercontinuum generation in chloroform-filled photonic crystal fibers. Optik **121**(9), 783–787 (2010). https://doi.org/10.1016/j.ijleo.2008.09.026

15. C.-C. Wang, W.-M. Li, N. Li, W.-Q. Wang, Numerical simulation of coherent visible-to-near-infrared supercontinuum generation in the CHCl3-filled photonic crystal fiber with 1.06 μm pump pulses. Opt. Laser Technol. **88**, 215–221 (2017). https://doi.org/10.1016/j.optlastec.2016.09.020

16. L.C. Van, V.T. Hoang, V.C. Long, K. Borzycki, K.D. Xuan, V.T. Quoc, M. Trippenbach, R. Buczyński, J. Pniewski, Optimization of optical properties of photonic crystal fibers infiltrated with chloroform for supercontinuum generation. Laser Phys. **29**(7), 075107 (2019). https://doi.org/10.1088/1555-6611/ab2115

17. F. Dai, Xu. Yonghao, X. Chen, Enhanced and broadened SRS spectra of toluene mixed with chloroform in liquid-core fiber. Opt. Express **17**(12), 19882–19886 (2009). https://doi.org/10.1364/OE.17.019882

18. R. Ahmad, M. Komanec, S. Zvanovec, Ultra-wideband mid-infrared supercontinuum generation in liquid-filled circular photonic crystal fiber. J. Nanophotonics **14**(2), 026016 (2020). https://doi.org/10.1117/1.JNP.14.026016

19. S. Junaid, J. Bierlich, A. Hartung, T. Meyer, M. Chemnitz, M.A. Schmidt, Supercontinuum generation in a carbon disulfide core microstructured optical fiber. Opt. Express **29**(13), 19891–19902 (2021). https://doi.org/10.1364/OE.426313

20. A. Sharafali, A.K. Shafeeque Ali, M. Lakshmanan, Modulation instability induced supercontinuum generation in liquid core suspended photonic crystal fiber with cubic-quintic nonlinearities. Phys. Lett. A **399**, 127290 (2021). https://doi.org/10.1016/j.physleta.2021.127290

21. A. Sharafali, K. Nithyanandan, A theoreticalstudy on the supercontinuum generation in a novel suspended liquid core photonic crystal fiber. Appl. Phys. B **126**(4), 55 (2020). https://doi.org/10.1007/s00340-020-7403-9

22. Q.H. Dinh, J. Pniewski, H.L. Van, A. Ramaniuk, V.C. Long, K. Borzycki, K.D. Xuan, M. Klimczak, R. Buczyński, Optimization of optical properties of photonic crystal fibers infiltrated with carbon tetrachloride for supercontinuum generation with sub-nanojoule femtosecond pulses. Appl. Opt. **57**(14), 3738–3746 (2018). https://doi.org/10.1364/AO.57.003738

23. V.T. Hoang, R. Kasztelanic, G. Stępniewski, K.D. Xuan, V.C. Long, M. Trippenbach, M. Klimczak, R. Buczyński, J. Pniewski, Femtosecond supercontinuum generation around 1560 nm in hollow-core photonic crystal fibers filled with carbon tetrachloride. Appl. Opt. **59**(12), 3720–3725 (2020). https://doi.org/10.1364/AO.385003

24. V.T. Hoang, R. Kasztelanic, A. Filipkowski, G. Stępniewski, D. Pysz, M. Klimczak, S. Ertman, V.C. Long, T.R. Woliński, M. Trippenbach, K.D. Xuan, M. Śmietana, R. Buczyński, Supercontinuum generation in an all-normal dispersion large core photonic crystal fiber infiltrated with carbon tetrachloride. Opt. Mater. Express **9**(5), 2264–2278 (2019). https://doi.org/10.1364/OME.9.002264

25. M. Chemnitz, C. Gaida, M. Gebhardt, F. Stutzki, J. Kobelke, A. Tünnermann, J. Limpert, M.A. Schmidt, Carbon chloride-core fibers for soliton mediated supercontinuum generation. Opt. Express **26**(3), 3221–3235 (2018). https://doi.org/10.1364/OE.26.003221

26. H.V. Le, V.T. Hoang, H.T. Nguyen, V.C. Long, R. Buczynski, R. Kasztelanic, Supercontinuum generation in photonic crystal fbers infltrated with tetrachloroethylene. Opt. Quantum Electron. **53**, 187 (2021). https://doi.org/10.1007/s11082-021-02820-3

27. L.C. Van, V.T. Hoang, V.C. Long, K. Borzycki, K.D. Xuan, V.T. Quoc, M. Trippenbach, R. Buczyński, J. Pniewski, Supercontinuum generation in photonic crystal fibers infiltrated with nitrobenzene. Laser Phys. **30**(3), 035105 (2020). https://doi.org/10.1088/1555-6611/ab6f09

28. Y. Guo, J.-H. Yuan, K. Wang, H. Wang, Y. Cheng, X. Zhou, B. Yan, X. Sang, Yu. Chongxiu, Generation of supercontinuum and frequency comb in a nitrobenzene-core photonic crystal fiber with all-normal dispersion profile. Opt. Commun. **481**, 126555 (2021). https://doi.org/10.1016/j.optcom.2020.126555

29. H.V. Le, V.L. Cao, H.T. Nguyen, A.M. Nguyen, R. Buczyński, R. Kasztelanic, Application of ethanol infiltration for ultra-flattened normal dispersion in fused silica photonic crystal fibers. Laser Phys. **28**(11), 115106 (2018). https://doi.org/10.1088/1555-6611/aad93a

30. Xu. Yonghao, X. Chen, Yu. Zhu, Modeling of micro-diameter-scale liquid core optical fiber filled with various liquids. Opt. Express **16**(12), 9205–9212 (2008). https://doi.org/10.1364/OE.16.009205

31. B.T. Le Tran, T.N. Thi, N.V.T. Minh, T. Le Canh, M. Le Van, V.C. Long, K.D. Xuan, L.C. Van, Analysis of dispersion characteristics of solid-core PCFs with different types of lattice in the claddings infiltrated with ethanol. Photonic Lett. Pol. **12**(4), 106–108 (2020). https://doi.org/10.4302/plp.v12i4.1054

32. P. Chauhan, A. Kumar, Y. Kalra, Supercontinuum generation in a hollow-core methanol-silica based photonic crystal fiber: computational model and analysis. In: Proc. SPIE 11498, Photonic Fiber and Crystal Devices: Advances in Materials and Innovations in Device Applications XIV 114980T (2020) https://doi.org/10.1117/12.2568970

33. P. Chauhan, A. Kumar, Y. Kalra, Ultra-coherent supercontinuum generation in isopropanol-silica based photonic crystal fiber at 1300nm and 1600nm wavelengths. In: Proc. SPIE 11289, Photonic and Phononic Properties of Engineered Nanostructures X 1128923 (2020). https://doi.org/10.1117/12.2544242.

34. R. Raei, M. Ebnali-Heidari, H. Saghaei, Supercontinuum generation in organic liquid-liquid core-cladding photonic crystal fiber in visible and near-infrared regions. J. Opt. Soc. Am. B **35**(2), 323–330 (2018). https://doi.org/10.1364/JOSAB.35.000323

35. J. Pniewski, T. Stefaniuk, H. Le Van, V.C. Long, L.C. Van, R. Kasztelanic, G. Stępniewski, A. Ramaniuk, M. Trippenbach, R. Buczyński, Dispersion engineering in nonlinear soft glass photonic crystal fibers infiltrated with liquids. Appl. Opt. **55**(19), 5033–5040 (2016). https://doi.org/10.1364/AO.55.005033t

36. A. Bozolan, C.J.S. de Matos, C.M.B. Cordeiro, E.M. dos Santos, J. Travers, Supercontinuum generation in a water-core photonic crystal fiber. Opt. Express **16**(13), 9671–9676 (2008). https://doi.org/10.1364/OE.16.009671

37. L. Tian, Li. Wei, F. Guoying, Numerical simulation of supercontinuum generation in liquid-filled photonic crystal fibers with a normal flat dispersion profile. Opt. Commun. **334**, 196–202 (2015). https://doi.org/10.1016/j.optcom.2014.07.080

38. K.D. Xuan, L.C. Van, V.C. Long, Q.H. Dinh, L.V. Xuan, M. Trippenbach, R. Buczynski, Dispersion characteristics of a suspended-core optical fiber infiltrated with water. Appl. Opt. **56**(4), 1012–1019 (2017). https://doi.org/10.1364/AO.56.001012

39. R. Zhang, J. Teipel, H. Giessen, Theoretical design of a liquid-core photonic crystal fiber for supercontinuum generation. Opt. Express **14**(15), 6800–6812 (2006). https://doi.org/10.1364/OE.14.006800

40. S. Das, M. DeVinod, K. Singh, Single mode dispersion shifted photonic crystal fiber with liquid core for optofluidic applications. Opt. Fiber Technol. **53**, 102012 (2019). https://doi.org/10.1016/j.yofte.2019.102012

41. K.L. Corwin, N.R. Newbury, J.M. Dudley, S. Coen, S.A. Diddams, K. Weber, R.S. Windeler, Fundamental noise limitations to supercontinuum generation in microstructure fiber. Phys. Rev.

Lett. **90**(11), 113904 (2003). https://doi.org/10.1103/PhysRev Lett.90.113904

42. A. Demircan, U. Bandelow, Analysis of the interplay between soliton fssion and modulation instability in supercontinuum generation. Appl. Phys. B **86**, 31–39 (2007). https://doi.org/10.1007/s00340-006-2475-8

43. K. Qian, Z. Gu, J. Xu, X. Dong, W. Yu, Z. Yu, D. Ren, Noise-like pulse erbium-doped fiber laser for supercontinuum generation. Optik **158**, 215–219 (2018). https://doi.org/10.1016/j.ijleo.2017.12.092

44. M. Klimczak, G. Soboń, R. Kasztelanic, K.M. Abramski, R. Buczyński, Direct comparison of shot-to-shot noise performance of all normal dispersion and anomalous dispersion supercontinuum pumped with sub-picosecond pulse fiber-based laser. Sci. Rep. **6**, 19284 (2016). https://doi.org/10.1038/srep19284

45. I.B. Gonzalo, R.D. Engelsholm, M.P. Sørensen, O. Bang, Polarization noise places severe constraints on coherence of all-normal dispersion femtosecond supercontinuum generation. Sci. Rep. **8**, 6579 (2018). https://doi.org/10.1038/s41598-018-24691-7

46. A.M. Heidt, J.S. Feehan, J.H.V. Price, T. Feurer, Limits of coherent supercontinuum generation in normal dispersion fibers. J. Opt. Soc. Am. B **34**(4), 764–775 (2017). https://doi.org/10.1364/JOSAB.34.000764

47. S. Kedenburg, M. Vieweg, T. Gissibl, H. Giessen, Linear refractive index and absorption measurements of nonlinear optical liquids in the visible and near-infrared spectral region. Opt. Mater. Express **2**(11), 1588–1611 (2012). https://doi.org/10.1364/OME.2.001588

48. D. Pysz, I. Kujawa, R. Stępień, M. Klimczak, A. Filipkowski, M. Franczyk, L. Kociszewski, J. Buźniak, K. Haraśny, R. Buczyński, Stack and draw fabrication of soft glass microstructured fiber optics. Bull. Pol. Acad. Sci. Tech. Sci. **62**(4), 667–682 (2014). https://doi.org/10.2478/bpasts-2014-0073

49. G. Fanjoux, S. Margueron, J.C. Beugnot, T. Sylvestre, Supercontinuum generation by stimulated Raman-Kerr scattering in a liquid-core optical fiber. J. Opt. Soc. Am. B **34**(8), 1677–1683 (2017). https://doi.org/10.1364/JOSAB.34.001677

50. V.T. Hoang, R. Kasztelanic, A. Anuszkiewicz, G. Stepniewski, A. Filipkowski, S. Ertman, D. Pysz, T. Wolinski, K.D. Xuan, M. Klimczak, R. Buczynski, All-normal dispersion supercontinuum generation in photonic crystal fibers with large hollow cores infiltrated with toluene. Opt. Mater. Express **8**(11), 3568–3582 (2018). https://doi.org/10.1364/OME.8.003568

51. L.C. Van, A. Anuszkiewicz, A. Ramaniuk, R. Kasztelanic, K.D. Xuan, V.C. Long, M. Trippenbach, R. Buczyński, Supercontinuum generation in photonic crystal fibres with core filled with toluene. J. Opt. **19**(12), 125604 (2017). https://doi.org/10.1088/2040-8986/aa96bc

52. Y. Sharma, R. Zafar, S. Kalra, G. Singh, Toluene-filled photonic crystal fiber with flat dispersion. In: Materialstoday: Proceedings **30**(1), 210–213 (2020). https://doi.org/10.1016/j.matpr.2020.06.109

53. S. Qiu, J. Yuan, X. Zhou, Qu. Yuwei, B. Yan, Wu. Qiang, K. Wang, X. Sang, K. Long, Yu. Chongxiu, Highly sensitive temperature sensing based on all-solid cladding dual-core photonic crystal fiber filled with the toluene and ethanol. Opt. Commun. **477**, 126357 (2020). https://doi.org/10.1016/j.optcom.2020.126357

54. Y.E. Monfared, C. Liang, R. Khosravi, B. Kacerovska, Selectively toluene-filled photonic crystal fiber sagnac interferometer with high sensitivity for temperature sensing applications. Res. Phys. **13**, 102297 (2019). https://doi.org/10.1016/j.rinp.2019.102297

55. K. Saitoh, M. Koshiba, T. Hasegawa, E. Sasaoka, Chromatic dispersion control in photonic crystal fibers: application to ultra-flattened dispersion. Opt. Express **11**(8), 843–852 (2003). https://doi.org/10.1364/OE.11.000843

56. K. Moutzouris, M. Papamichael, S.C. Betsis, I. Stavrakas, G. Hloupis, D. Triantis, Refractive, dispersive and thermo-optic properties of twelve organic solvents in the visible and near-infrared. Appl. Phys. B **116**(3), 617–622 (2013). https://doi.org/10.1007/s00340-013-5744-3

57. C.Z. Tan, Determination of refractive index of silica glass for infrared wavelengths by IR spectroscopy. J. Non-Cryst. Solids **223**(1–2), 158–163 (1998). https://doi.org/10.1016/s0022-3093(97)00438-9

58. https://www.lumerical.com/products/mode.

59. J.M. Dudley, J.R. Taylor, *Supercontinuum generation in optical fibers* (Cambridge University Press, Cambridge, 2010)

60. C. Finot, B. Kibler, L. Provost, S. Wabnitz, Beneficial impact of wave-breaking for coherent continuum formation in normally dispersive nonlinear fibers. J. Opt. Soc. Am. B **25**(11), 1938–1948 (2008). https://doi.org/10.1364/JOSAB.25.001938